The DIC carbon isotope evolutions during CO_2 bubbling: implications for ocean acidification laboratory culture

Hongrui Zhang[1], Ismael Torres-Romero[1], Pien Anjewierden[1], Madalina Jaggi[1], Heather M. Stoll[1]

[1] Climate Geology, Department of Earth Sciences, ETH Zürich, Sonneggstrasse 5, 8092 Zurich, Switzerland

Abstract

Ocean acidification increases pCO_2 and decreases pH of seawater and its impact on marine organisms has emerged as a key research focus. In addition to directly measured variables such as growth or calcification rate, stable isotopic tracers such as carbon isotopes have also been used to more completely understand the physiological processes contributing to the response of organisms to ocean acidification. To simulate ocean acidification in laboratory cultures, direct bubbling of seawater with CO_2 has been a preferred method because it adjusts pCO_2 and pH without altering total alkalinity. Unfortunately, the carbon isotope equilibrium between seawater and CO_2 gas has been largely ignored so far. Frequently, the dissolved inorganic carbon (DIC) in the initial seawater culture has a distinct $^{13}C/^{12}C$ ratio which is far from the equilibrium expected with the isotopic composition of the bubbled CO_2. To evaluate the consequences of this type of experiment for isotopic work, we measured the carbon isotope evolutions in two chemostats during CO_2 bubbling and composed a numerical model to simulate this process. The isotopic model can predict well the carbon isotope ratio of dissolved inorganic carbon evolutions during bubbling. With help of this model, the carbon isotope evolution during a batch and continuous culture can be traced dynamically improving the accuracy of fractionation results from laboratory culture. Our simulations show that if not properly accounted for in experimental or sampling design, many typical culture configurations involving CO_2 bubbling can lead to large errors in estimated carbon isotope fractionation between seawater and biomass or biominerals, consequently affecting interpretations and hampering comparisons among different experiments. Therefore, we describe the best practices on future studies working with isotope fingerprinting in the ocean acidification background.

1. Introduction

The ocean acidification problem is becoming more and more serious with the continuous increase of atmosphere CO_2 from fossil fuel burning. Ocean acidification can be defined as the

increase of dissolved CO_2 ($CO_{2(aq)}$) and consequent decrease of pH in seawater, with increase of dissolved inorganic carbon (DIC) but little variations in total alkalinity (Gattuso and Hansson, 2011). In the last two decades, thousands of studies have been carried out to study the ocean acidification effects on different marine organisms which have been reviewed and synthesized (e.g.Hoegh-Guldberg et al., 2007; Lemasson et al., 2017; Meyer and Riebesell, 2015; Riebesell and Tortell, 2011). These studies have shown that ocean acidification has complex effects on marine calcifiers (Figuerola et al., 2021), non-calcifying marine life (Hurd et al., 2019), and therefore profound impact on marine ecosystem and ocean carbon cycles (Mostofa et al., 2016). Over the past decade, more studies have employed isotopic methods in laboratory cultures, to trace the ratio of stable isotopes, whose variations reveal important physiological responses to ocean acidification beyond, for instance, growth rate, cell size, or elemental stoichiometry, and also calibrate new proxies for reconstructing the atmospheric CO_2 concentration in geological history (Hopkinson et al., 2011; Nishida et al., 2020; Phelps et al., 2021; Remize et al., 2021; Wilkes et al., 2017).

Laboratory culture is a key method to study the physiological effect of ocean acidification on different marine life. There are multiple methods to achieve the target culture media $CO_{2(aq)}$ and carbonate chemistry depending on the objectives of the study. The principal methods are (1) manipulating pH by adding acid/base, (2) manipulating DIC through addition of HCO_3^- or CO_3^{2-} and (3) bubbling (or aeration) a gas of desired pCO_2 concentration (Gattuso et al., 2010) . The method of bubbling cultures with CO_2 requires a step of gas mixing to obtain the desired CO_2 level and humidification step preventing evaporation from cell culture media. Adding acid/base removes the mechanical stress upon cells from bubbles and benefits from relative easy operations, however it could cause trace metal concentration variation (Shi et al., 2009). Both of bubbling and acid-base manipulation can well simulate the CO_2 increase and pH decrease effects in laboratory culture, but the CO_2 bubbling method has been preferred by some studies because it alone can perfectly replicate the current ocean acidification caused by anthropogenic CO_2 without changing the seawater total alkalinity.

For the CO_2 bubbling method, the guidebook by Riebesell et al. (2011), covering the methods of laboratory culture for ocean acidification research, highlighted the importance of pre-equilibrating the culture media to the required CO_2 concentration by aerating it 'for a few days'. Considering the wide range of culture vessel shapes and volumes among experiments, our question is how long culture media should be bubbled in order to reach an ordinary chemical and isotopic balance. Some of published works mentioned the pre-bubbling durations, for example, the seawater was pre-bubbled for 2 days Iglesias-Rodriguez et al.

(2008), while most of publications did not fully describe their methods. Moreover, the isotopic equilibration times are usually much longer than the ordinary chemical equilibration times, because, to reach isotopic equilibrium, each ion and molecule should be fully exchanged and come to equilibrium with other ions and molecules (Mills and Urey, 1940). For the works focusing on organic or carbonate carbon isotope fractionations under different CO_2 levels, culture media with out of equilibrium or dynamic carbon isotope ratio of DIC could complicate or even preclude the interpretation of stable isotope fractionation signatures.

In this study, we provide a thorough characterization of the isotopic equilibration process in CO_2 bubbling experiments and the factors that influence the carbon isotopic equilibration time, in order to clearly document the approaches needed to accurately infer carbon isotopic fractionations in experiments with bubbling. First, we compose numerical models to simulate chemical and isotopic equilibration during bubbling processes in two different systems and present the effects of DIC volume, gas exchange rate, and isotopic difference between bubbled CO_2 and un-bubbled DIC on the equilibration time. Secondly, we complete a series of bubbling experiments in a photobioreactor to test the performance of the model simulation. Finally, we evaluate the expected consequences of equilibration time in typical experimental bubbling setups for which carbon isotopic ratio of cultured biomass or biominerals have been reported. With help of this study, future works can trace the isotopic fingerprint of ocean acidification on marine biomass better.

2. Experimental setup for determination of equilibration time

We have conducted experiments in commercial photobioreactors of 1L and 3L (PBR FMT 150, Photon Systems International). designed for continuous culture. The aeration system allowed gas to first enter the bottom of a bottle with fresh medium ('bottle' in **Figure 1a**), where gas humidification and the first exchange of gases occurred. The gas subsequently flowed out towards the photobioreactor where a sparging tube dispersed the bubbles, exchanging gases a second time. Finally, gas flowed to the waste bottle, and from there out of the system (**Figure 1a**). The photobioreactor compartments were monitored without inoculated cells in batch mode in order to assess the dynamics of the bubbling process itself. The two different photobioreactor sizes and CO_2 concentrations employed in this study can be found in **Table 1**.

For the different CO_2 concentration treatments, two compressed gases, pure CO_2 with a $\delta^{13}C$ of -2.8‰ (Vienna Pee Dee Belemnite, VPDB) and CO_2-free synthetic air (Air Liquide), were mixed with a Gas Mixing System (GMS-150, Photon Systems Instruments). GMS output flow and pCO_2 composition were further verified with a flowmeter and a cavity ringdown

spectrometer isotopic and gas concentration analyzer (G2131-*i*, Picarro, Inc. USA). Measurements of the Picarro CO_2 analyzer were corrected with CO_2 mixtures with certified concentrations and isotopic composition (Air Liquide). Photobioreactors were filled with K/2 medium (Keller et al., 1987) without Tris buffer. Prior to filtration, artificial seawater (ASW) was supplemented with Na_2CO_3 and HCl to raise alkalinity above 4 mmol kg^{-1} seawater.

DIC in media was monitored with an Apollo SciTech DIC-C13 Analyzer coupled to the Picarro CO_2 analyzer using in-house $NaHCO_3$ standards dissolved in deionized water at different known concentrations and $\delta^{13}C$ values from -4.66 to -7.94‰. $\delta^{13}C$-DIC in media were measured with a Gas Bench II with an autosampler (CTC Analytics AG, Switzerland) coupled to ConFlow IV Interface and a Delta V Plus mass spectrometer (Thermo Fischer Scientific). The system and abovementioned in-house standards were calibrated using international standards NBS 18 (-5.014‰), NBS 19 (+1.95‰) and LSVEC (-46.6‰). The analytical error for $CO_{2(g)}$ concentration is <20 ppm and that for DIC concentration and $\delta^{13}C$ is <10 µM and 0.1‰, respectively.

Our initial $\delta^{13}C$ of un-bubbled DIC (at t_0) is -6.1±0.2‰. Before and after the start of bubbling at a flow of 200±20 mL min^{-1}, both headspace and seawater medium of the upstream bottle and the photobioreactor were sampled by a 50-mL syringe through one-way sampling ports. The sampling time in each experiment can be found in **Table 2**. To measure headspace $CO_{2(g)}$ that had been humidified and exchanged with bottle medium, gas flow was directed into a syringe and 50 mL of gas were injected into the Picarro CO_2 analyzer. To measure seawater DIC, pH and $\delta^{13}C_{DIC}$, 35 mL seawater were syringed out as depicted in **Figure 1a**. The first 5-10 mL out of 35 mL were routinely discarded to avoid mixing effects with dead volumes in the tubing. One mL was injected into He-flushed glass vials containing H_3PO_4 for the Gas Bench, 3.5 mL into the Apollo analyzer, in duplicate and the remaining was taken for pH measurement using a pH-probe calibrated with NBS standards (Mettler Toledo).

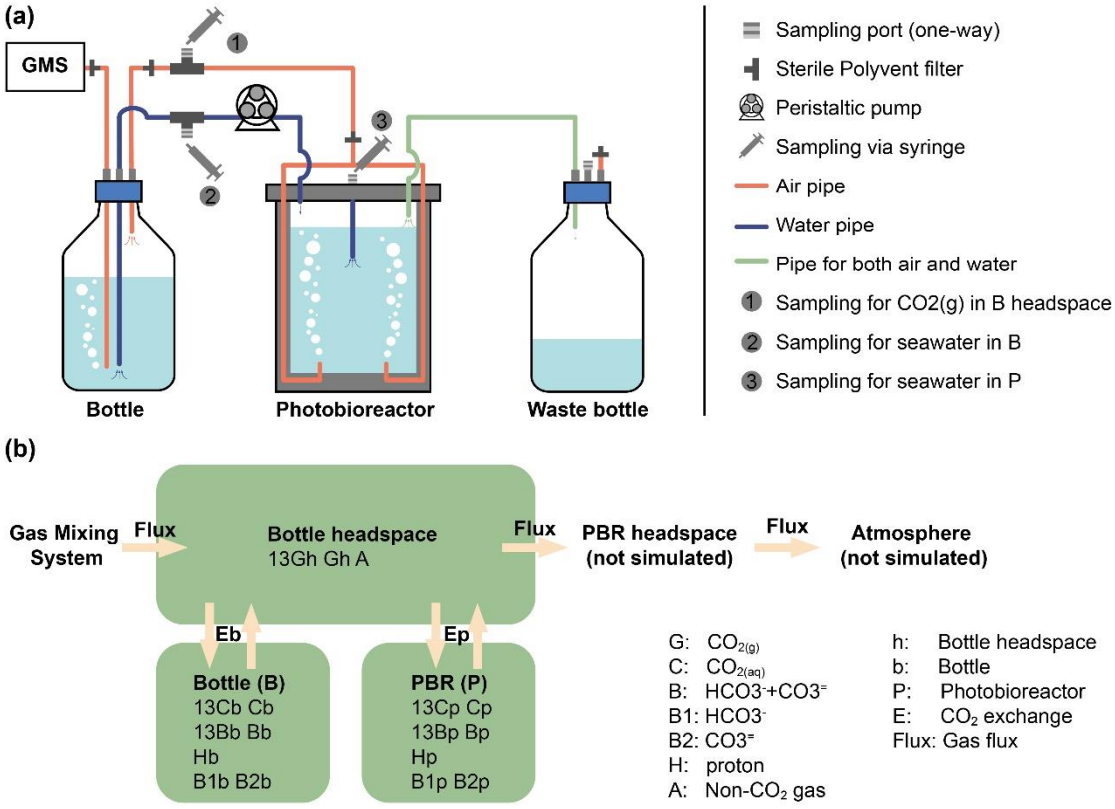

Figure 1. The photobioreactor system with CO_2 bubbling and model structure. **(a)** The photobioreactor system in Climate Geology laboratory, ETH Zurich. GMS means Gas Mixing System. **(b)** Our model consists of three compartments: bottle headspace, bottle media and photobioreactor media (words in bold). PBR is the photobioreactor. The other terms are simulated amount/concentration of substance, in which capital letters represent substance and subscript letters are abbreviation for compartments.

Table 1. Parameters for photobioreactor systems

	Seawater volume (L)	Headspace volume (L)	k_E (mol s^{-1} atm^{-1})	Gas flux (mL min^{-1})	CO_2 (ppm atm)
Large system					
Bottle	2	~0.2	8.71E-05	200	2350
Photobioreactor	3.1	_	4.57E-05		
Small system					
Bottle	0.9	~0.1	5.32E-05	200	470
Photobioreactor	0.95	_	3.36E-05		

Table 2. DIC and $CO_{2(g)}$ in headspace measurements during small system bubbling

Time (h)	Bottle			Photobioreactor			Bottle headspace	
	[DIC] (µM)	$\delta^{13}C_{DIC}$ (‰, VPDB)	pH (NBS)	[DIC] (µM)	$\delta^{13}C_{DIC}$ (‰, VPDB)	pH (NBS)	pCO_2 (ppm atm)	$\delta^{13}C_{CO2(g)}$ (‰, VPDB)
0.00	4122	-6.07	8.08	4079	-6.54	7.80	882	-13.46
0.08							616	-7.32
0.30	3769						792	
0.48		-5.94	8.11	4022	-6.60	8.01		
0.58							598	-6.74
1.50	3727	-5.68	8.16		-6.27	8.01	556	-6.68
2.42							528	-6.32
3.50	3652	-5.06	8.18	3834	-5.97	8.13		
4.00							506	-5.87
6.00	3614	-4.35	8.28	3753	-5.57	8.23		
6.17							499	-5.60
9.00	3590	-3.79	8.30	3696	-5.04	8.26	473	-5.86
15.92	3582	-2.33	8.29	3660	-3.77	8.31		
18.92	3558	-1.53	8.31	3650	-3.29	8.33		
21.83	3576	-1.09	8.29	3639	-2.87	8.32		
24.75	3556	-0.67	8.30	3646	-2.33	8.33		
46.92	3578	1.39	8.31	3630	0.37	8.35		
71.00	3612	3.60	8.32	3627	2.52	8.36		
97.00	3621	4.30	8.35	3606	3.88	8.36		
124.42		5.40	8.35		5.49	8.36		
125.25							475	-2.80
171.08		5.51	8.35		5.66	8.36		

Table 3. DIC and $CO_{2(g)}$ in headspace measurements during large system bubbling

Time (h)	Bottle			Photobioreactor			Bottle headspace	
	[DIC] (µM)	$\delta^{13}C_{DIC}$ (‰, VPDB)	pH (NBS)	[DIC] (µM)	$\delta^{13}C_{DIC}$ (‰, VPDB)	pH (NBS)	pCO_2 (ppm atm)	$\delta^{13}C_{CO2(g)}$ (‰, VPDB)
0.00		-5.65	8.09	3844	-6.06	8.09	944	-15.31
0.08							1957	-4.31
0.32							2009	-4.22
0.50		-5.51	8.02	3866	-5.97	8.02		
0.63							2001	-4.53
1.17							2066	-4.80
1.50		-5.10	7.90	3893	-5.93	7.90		
2.75							2248	-5.09
3.50		-4.22	7.78	3970	-5.93	7.78		
5.08							2331	-5.46
6.00		-3.27	7.75	4017	-5.22	7.75		-1.30
7.42							2328	-5.52
8.53							2340	-5.32
8.67	4181	-2.17	7.77	4036	-4.79	7.77		
15.42	4172	-0.15	7.78	4036	-3.37	7.78		
18.33	4176	0.51	7.79	4029	-2.75	7.79		
21.42	4152	1.49	7.77	4044	-2.27	7.77		
24.25	4186	1.66	7.79	4035	-1.64			
46.42	4031	4.19	7.84	4026	1.78			
70.50	4041	5.03	7.81	4031	3.97			
96.00	4029	5.11	7.77	3993	4.93			
123.33		5.28	7.77					
125.03							2421	-2.81
170.75		5.52	7.81		5.46			

3. Approach for simulating the gas bubbling process in a numerical model

There are three important processes in DIC carbon isotope evolution simulations, (1) CO_2 exchanging between gas ($CO_{2(g)}$) and seawater ($CO_{2(aq)}$), (2) DIC inter-reactions and (3) isotopic fractionation during the DIC reactions, which will be introduced separately in the following sections. Beside these three main processes, the sampling of DIC and gas in headspace can also play a minor role in DIC isotope evolution by decreasing the total amount of DIC and accelerating isotopic equilibrium. Thus, the decreasing of DIC volume and the loses of $CO_{2(g)}$ in headspace during sampling are also considered in our model. As described in the last section, the CO_2 coming from the Gas Mixing System first goes into the bubbling in bottle, exchanging with DIC in bottle. Then $CO_{2(g)}$ goes out of the seawater in bottle into the bottle

headspace. After that, $CO_{2(g)}$ goes into bubbles in photobioreactor exchanging with DIC in photobioreactor. However, in our model, bubbles in bottle and photobioreactor are combined with bottle headspace to reduce the calculation amount. Thereby, in practice, the simulated $CO_{2(g)}$ goes into headspace directly after flowing out of Gas Mixing System, and exchanges with DIC in bottle and photobioreactor together (**Figure 1b**). With these simplifications, there are only two degrees of freedom in our model: CO_2 exchange rate constants (k_E) in bottle and photobioreactor. Using a given combination of k_E, the forward model runs ordinary differential equations (ODEs) toward steady state using the Matlab function 'ode15s', with seawater and $CO_{2(g)}$ composition in bottle, photobioreactor and bottle headspace as initial conditions. The notations and equations of the model are described in detail in the **Appendix A** and **B**, respectively. Fitting processes were carried out to estimate the exchange rate constants and gas flux. These processes were achieved by minimizing the difference between simulated carbon isotope ratios and measured values via the Matlab function 'fmincon'.

3.1 Exchanging between $CO_{2(g)}$ and $CO_{2(aq)}$

The equilibrium between $CO_{2(g)}$ in headspace and $CO_{2(aq)}$ in seawater follows Henry's law (Carroll et al., 1991). The net exchange rate (ER) between seawater and headspace follows the Fick's diffusion law:

$$\mathrm{ER} = D_{CO2} \times A \times \frac{d[CO_2]}{dx} \quad (1)$$

where the D_{CO2} is the diffusion coefficient which depends on temperature and pressure, A is the surface area and $\frac{d[CO_2]}{dx}$ is the CO_2 concentration gradient between seawater and headspace. In a bubbling system, the surface area depends on the number and size of bubbles, which are difficult to estimate (e.g. Martínez and Casas, 2012). Here, to simply our model, we define an exchange rate constant into the **Eq. 1**, which is a function of bubble surface area, temperature and pressure. If the exchange flux from gas phase into seawater is defined as positive, then net CO_2 exchange rate between gas and seawater can be described by k_E (with a unit of mol s^{-1} atm^{-1} in this case) and the CO_2 concentration difference between headspace and seawater by the following equation:

$$\mathrm{ER} = k_E \times \left([pCO_{2h}] - \left[CO_{2aq}\right]/k_H\right) \quad (2)$$

where the k_H is the Henry's Law constant, which depends on temperature and is 0.035 mol L^{-1} atm^{-1} at T =291.15K for this work. The pCO_{2h} is the CO_2 concentration in headspace, with a unit of atm. The $CO_{2(aq)}$ is the CO_2 concentration in seawater, with a unit of mol L^{-1}. Since the

k_E is difficult to calculate directly, we can estimate it by tracing the DIC carbon isotope evolution during bubbling, which will be described in **Section 4.1**.

3.2 DICs inter-reactions

The DICs inter-reactions in the seawater include:

$$CO_{2(aq)} + H_2O \overset{k_{+1}/k_{-1}}{\Longleftrightarrow} H^+ + HCO_3^- \quad (3)$$

$$CO_{2(aq)} + OH^- \overset{k_{+4}/k_{-4}}{\Longleftrightarrow} HCO_3^- \quad (4)$$

$$CO_3^{2-} + H^+ \overset{k^H_{+5}/k^H_{-5}}{\Longleftrightarrow} HCO_3^- \quad (5)$$

$$CO_3^{2-} + H_2O \overset{k^{OH}_{+5}/k^{OH}_{-5}}{\Longleftrightarrow} HCO_3^- + OH^- \quad (6)$$

The reaction rate constants follow definitions in Zeebe and Wolf-Gladrow (2001), where k_{+1} and k_{-1} are constants for hydration and dehydration reactions, k_{+4} and k_{-4} are for hydroxylation and dehydroxylation reactions and k_{+5} and k_{-5} are for CO_3^{2-} and HCO_3^- exchanging. To increase the simulation efficiency, the conversions between HCO_3^- and CO_3^{2-} are assumed to be instantaneous since they are about 8-9 orders of magnitudes higher than the reactions rate between $CO_{2(aq)}$ and HCO_3^- (Zeebe and Wolf-Gladrow, 2001). The hydrolysis reactions (**Eq. 6**) are not simulated in our model in order to increase the simulation efficiency, but the protolysis reactions (**Eq. 5**) are simulated to calculate H^+ concentration and thereby simulate the dynamic seawater pH during CO_2 bubbling.

3.3 Carbon isotope fractionations

The carbon isotope ratios of DIC and $CO_{2(g)}$ were shown as the relative abundance of $^{13}C/^{12}C$ in substance X ($^{13}R_x$) compared with the ratio of $^{13}C/^{12}C$ in standard carbonate ($^{13}R_{std}$, VPDB in this study):

$$\delta^{13}C_X = \left(\frac{^{13}R_X}{^{13}R_{std}} - 1\right) \times 1000 \quad (7)$$

The main processes causing isotopic fractionation in our simulations are: (1) $CO_{2(aq)}$-HCO_3^- inter-reactions and (2) CO_2 diffusion in air and CO_2 diffusion from gas phase into liquid phase. In our model, beside the concentrations of $CO_{2(g)}$, $CO_{2(aq)}$, HCO_3^- and CO_3^{2-}, the concentrations of $^{13}CO_{2(g)}$, $^{13}CO_{2(aq)}$, $H^{13}CO_3^-$ and $^{13}CO_3^{2-}$ are also calculated. Isotopic fractionations are simulated by using larger or smaller reaction rate constants following Zeebe and Wolf-Gladrow (2001). A summary of reaction rate constants and fractionation factors can be found

in **Appendix Table A1**. The reaction rates of DIC and $CO_{2(g)}$ with heavy carbon atoms are listed in **Eq. B1-B10**.

In this work, the $\delta^{13}C_{CO2(g)}$ is about -2.8‰. The carbon isotope fractionation between $CO_{2(g)}$ and $CO_{2(aq)}$ is about 1.2‰ ($CO_{2(g)}$ is less enrich of ^{13}C than $CO_{2(aq)}$). The fractionation between $CO_{2(aq)}$ and HCO_3^- is about -9.8‰ at 291.15K ($CO_{2(aq)}$ is more depleted in ^{13}C than HCO_3^-). The three DIC components vary with pH: the proportion of $CO_{2(aq)}$ decreases with increase of pH, while CO_3^{2-} increases with the concomitant increase of pH. Since the HCO_3^- is the dominant component in seawater DIC, the value of carbon isotope fractionation between $CO_{2(aq)}$ and HCO_3^- is close to the one between $CO_{2(aq)}$ and total DIC (~0.3‰ difference when pH is around 8, **Figure 2**). In conclusion, ignoring the fractionation in $CO_{2(g)}$ diffusion, the carbon isotope ratios of DIC should be about 8.3‰ more positive than that of $CO_{2(g)}$, when they are in equilibrium, at our culture temperature and pH. In other words, the DIC carbon isotope ratio should be around 5.5‰ after equilibrium with $CO_{2(g)}$ given a temperature of 291.15K and $\delta^{13}C_{CO2(g)}$= -2.8‰ for this work.

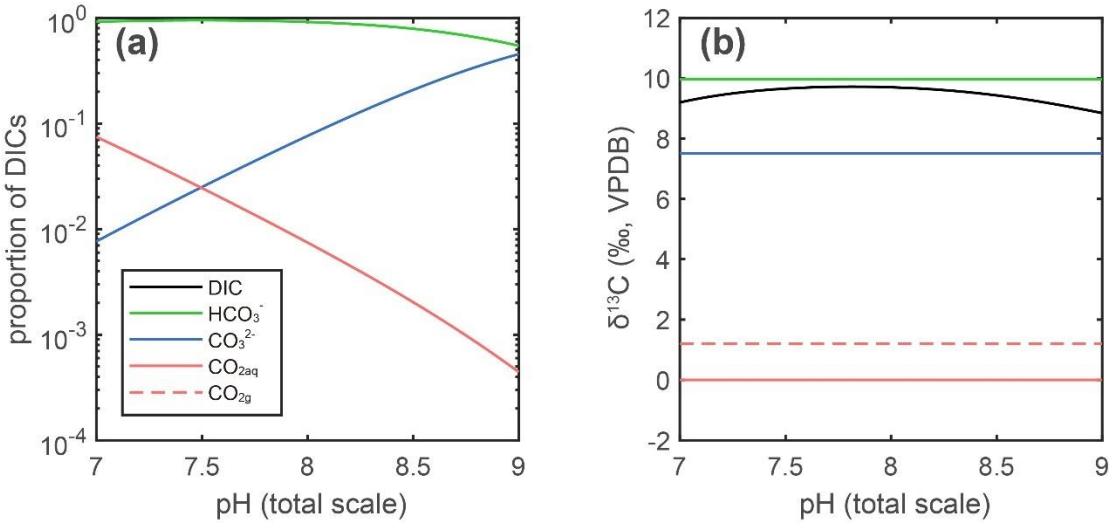

Figure 2. DIC proportion and isotope fractionation in different pH. **(a)** The ratio of the three components of DIC are plotted on a log scale in function of pH for a seawater at T = 291.15K and Salinity = 35‰. **(b)** The isotopic fractionations are calculated by the parameters in **Table A1.** The $\delta^{13}C_{VPDB}$ of $CO_{2(aq)}$ is arbitrarily set as 0‰ (red line). In isotopic equilibrium, the $CO_{2(g)}$ is heavier than $CO_{2(aq)}$ by 1.2‰, the HCO_3^- is heavier than $CO_{2(aq)}$ by 9.8‰ and CO_3^{2-} is heavier than $CO_{2(aq)}$ by 7.4‰ (Zhang et al., 1995). The fractionation between total DIC and $CO_{2(aq)}$ is a function of pH as it determines the proportion of each DIC.

4. Results of simulations of the DIC evolution in bubbling

In this study, we carried out two experiments to estimate the CO_2 exchange rate constants between gas and seawater. The fitting results of CO_2 exchange rate constant (k_E) are 8.71×10^{-5}, 4.57×10^{-5}, 5.32×10^{-5} and 3.36×10^{-5} mol s^{-1} atm^{-1} for large system bottle, large system photobioreactor, small system bottle and small system photobioreactor, respectively.

The $\delta^{13}C_{DIC}$ before bubbling are around -6.1‰ (-6.54~-5.65‰). With the onset of bubbling, $\delta^{13}C_{DIC}$ responded logarithmically, increasing fastest during the first hours and slowing the rate of increase in the following days. The $\delta^{13}C_{DIC}$ in both experiments did not increase further after reaching values around 5.5 ‰, about 8.3 ‰ higher than the $CO_{2(g)}$, which well fitted our prediction in the last section. The $\delta^{13}C_{DIC}$ reached equilibrium with $CO_{2(g)}$ at 6 days in low CO_2 experiment with pCO_2 = 470ppm, while in the other experiment, the isotopic equilibrium was achieved at 5 days after bubbling. In our simulations, the carbon exchange rate between $CO_{2(aq)}$ and HCO_3^- is more than two order of magnitude higher than the rate between $CO_{2(g)}$ and $CO_{2(aq)}$. Therefore, carbon isotope ratios of $CO_{2(aq)}$ ($\delta^{13}C_{CO2(aq)}$) are almost parallel with $\delta^{13}C_{DIC}$ (dashed lines in **Figure 3**).

Compared to the continually increasing $\delta^{13}C_{DIC}$ and $\delta^{13}C_{CO2(aq)}$, the carbon isotope ratio of CO_2 gas ($\delta^{13}C_{CO2(g)}$) in bottle headspace interestingly showed more variations (blue dots in **Figure 3**). The initial value of $\delta^{13}C_{CO2(g)}$ was around -15‰, which is the atmosphere CO_2 carbon isotope ratio in the poorly ventilated laboratory. There were sharp increases in $\delta^{13}C_{CO2(g)}$ from -15‰ to around -6‰, immediately after bubbling (-4.31‰ in high pCO_2 experiment and -7.32‰ in low pCO_2 experiment, only five minutes after bubbling). This was caused by the CO_2 in bottle headspace being rapidly replaced by the new CO_2 coming from the Gas Mixing System, which has a carbon isotope fingerprint of -2.8‰. With a fixed gas flux, this kind of rapid increase in $\delta^{13}C_{CO2(g)}$ was more significant in high CO_2 concentration experiment (**Figure 3b**). The rapid increase of $\delta^{13}C_{CO2(g)}$ was then followed by a decrease of $\delta^{13}C_{CO2(g)}$, which was caused by CO_2 exchanging between gas in headspace and DIC in seawater. In the large system, the CO_2

exchange rate is about 640% higher than the rate in small system, due to the higher pCO_2 and higher k_E. Therefore, the ^{13}C in $CO_{2(g)}$ went into DIC in seawater faster in the larger system, resulting an about 1.2‰ decline in $\delta^{13}C_{CO2(g)}$ and also faster increases in $\delta^{13}C_{DIC}$ (**Figure 3b**). This complex pattern of $\delta^{13}C_{CO2(g)}$ was well simulated in our model (blue lines in **Figure 3**), though the simulation results are a bit lower value than measurements in high CO_2 experiment. This could be caused by combination of the bubbles in bottle and photobioreactor with the headspace in our model, resulting a more significant decline in $\delta^{13}C_{CO2(g)}$ when $CO_{2(g)}$ begins to exchange with DIC.

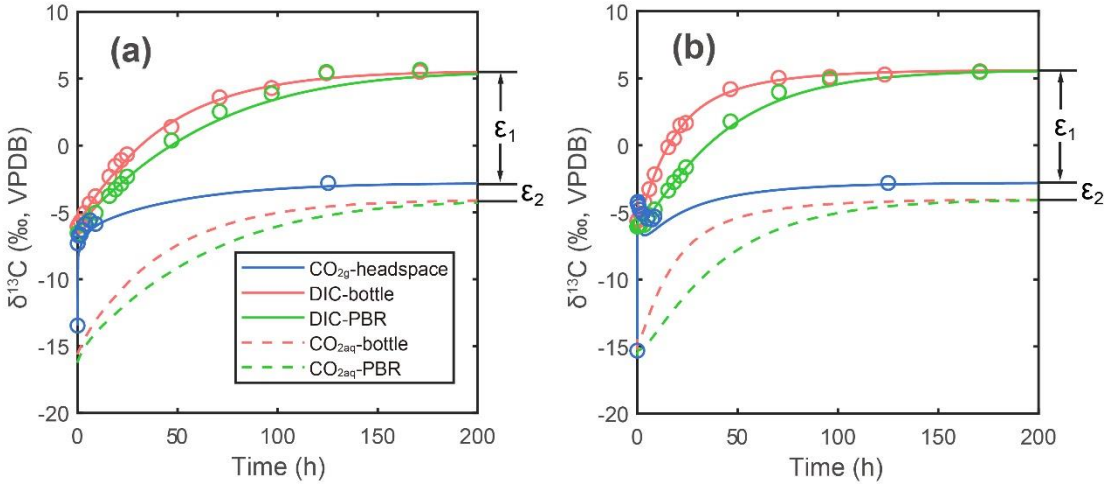

Figure 3. Measurements and simulations in two bubbling experiments: (a) lower CO_2 experiment in small photobioreactor system; (b) higher CO_2 experiment in large photobioreactor system. Lines are simulation results and dots are measured. Blue lines and dots are carbon isotope ratio of $CO_{2(g)}$ in headspace, red lines and dots are DIC carbon isotope in bottle and green lines and dots are DIC carbon isotope in photobioreactor (PBR in legend). Red and green dashed lines are simulated $CO_{2(aq)}$ carbon isotope ratios in bottle and photobioreactor, respectively. The ε_1 and ε_2 are carbon isotope fractionation between DIC and $CO_{2(g)}$ and $CO_{2(g)}$ and $CO_{2(aq)}$, respectively.

5. Implications for experimental setup and interpretation

5.1 Factors controlling equilibration time

To study the potential influence of equilibration time, a series of sensitivity tests are carried out by simulating the DIC evolution during bubbling in different settings. Here we define the '99% ordinary equilibration time' as the time when $[CO_{2(aq)}]$ reach $[CO_{2(aq)\ t=0}] + 0.99([CO_{2(aq)\ t=\infty}] - [CO_{2(aq)\ t=0}])$. Similarly, the '99% carbon isotopic equilibration time' is defined as the time when the DIC carbon isotope ratio reaches $\delta^{13}C_{DIC\ t=0} + 0.99(\delta^{13}C_{DIC\ t=\infty} - \delta^{13}C_{DIC\ t=0})$. The first

sensitivity test is on the effect of CO_2 gas exchange rate constant (k_E) on equilibration time. Given a DIC concentration of 2200 µM and in a media volume of 1 L, and the initial carbon isotope difference between $CO_{2(g)}$ and DIC of 5‰ ($\delta^{13}C_{CO2(g)}$ - $\delta^{13}C_{DIC\ t=0}$ = 5‰), both ordinary and isotopic equilibration time increase with a decreasing CO_2 exchange rate constant (**Figure 4a**). Hence, we suggest that the CO_2 exchange rate between gas and seawater is the first-order limitation of isotopic equilibration time.

In the second simulation, the effect of culture media volume (or total DIC amount) was tested. Given a DIC concentration of 2200 µM, an initial carbon isotope difference between $CO_{2(g)}$ and DIC ($\Delta_{t=0}$) as 5‰ ($\delta^{13}C_{CO2(g)}$ - $\delta^{13}C_{DIC\ t=0}$ = 5‰) and a k_E of 10^{-4} mol s^{-1} atm^{-1}, both of ordinary and isotopic equilibration time show a linear increase with the seawater volume (**Figure 4b**). These simulations fit the expectation that when the total DIC amount is higher, it will take longer to reach equilibrium in the system.

Finally, we evaluate the effect of initial carbon isotope difference between $CO_{2(g)}$ and DIC on equilibration time. The carbon isotope of $CO_{2(g)}$ was fixed in all simulations, but the initial carbon isotope ratio of DIC was varied, with initial carbon isotope difference ranging from -40 to 20‰. The DIC concentration was set as 2200 µM and the volume of medium at 1 L. The simulation results in **Figure 4c** show that when the $\Delta_{t=0}$ is around -8.3‰, which is the equilibrium fractionation between $CO_{2(g)}$ and DIC at T = 291.15K, the DIC reaches isotopic equilibrium with $CO_{2(g)}$ even faster than the ordinary chemistry equilibrium. When the absolute isotopic difference ($|\Delta_{t=0}|$) is larger, for example from -8.3 to -20‰, the isotopic equilibration time would increase exponentially. Another interesting observation is that when the isotopic difference between $CO_{2(g)}$ and DIC is large enough, the time to reach isotopic equilibrium will not increase with the $|\Delta_{t=0}|$. We suggest that this is the time cost for all carbon atoms in the DIC to fully exchange with carbon atoms in $CO_{2(g)}$.

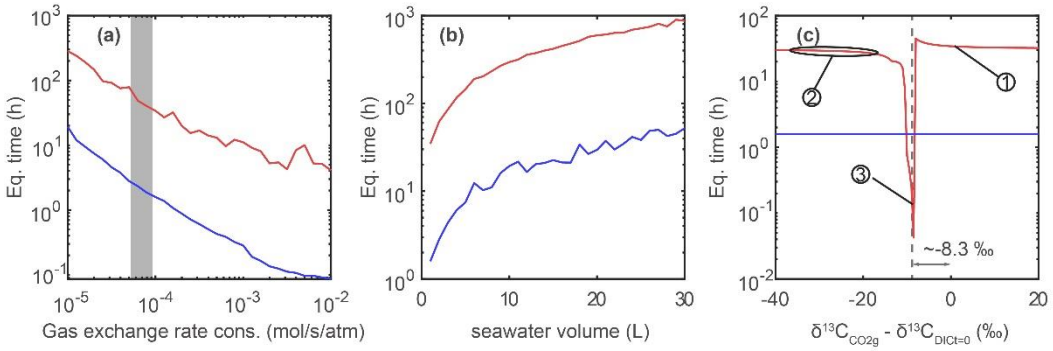

Figure 4. **Sensitivity tests of different parameters effects on equilibration time. (a)** Both isotopic (red) and ordinary (blue) equilibration times decrease with the increase of gas exchange rate constant. The grey shaded area represents the estimated gas exchange rate constants in this work, ranging from $10^{-4.4}$ to $10^{-4.1}$ mol s^{-1} atm^{-1}. **(b)** Both isotopic (red) and ordinary (blue) equilibration times increase with the increase of seawater volume. **(c)** The DIC carbon isotope reaches equilibrium faster when the carbon isotope ratio difference between DIC and $CO_{2(g)}$ is around 8.3‰ (same as the ε_1 in **Figure 3**), which is the equilibrium fractionation between DIC and $CO_{2(g)}$ at 291.15K. The carbon isotope difference does influence equilibration time especially when the difference is between -20‰ and -8.3‰. Numbering illustrates isotopic ratio differences in representative experiments here and in published works: No. 1 marks a $\Delta_{t=0}$ = 1.7‰ in k_E measurement experiments in this study. No. 2 marks $\Delta_{t=0}$ ranging from about -37 to -17‰ in several other works (e.g. Liu et al., 2018; Phelps et al., 2021). No. 4 marks a $\Delta_{t=0}$ around -9‰ (Tchernov et al., 2014).

5.2 Potential equilibration time effects in typical experimental setups

In recent years, more laboratory culture works have focused on carbon isotope variations in biogenic carbonate or bulk/special organic carbon under ocean acidification scenarios. We consider the expected behavior of carbon chemistry equilibration in three types of published experimental setups, and implications for the estimation of carbon isotope fractionation between DIC and biomass or biominerals.

5.2.1 Aeration of the gas surface without bubbling

The longest equilibration time would be expected for systems in which CO_2 is not bubbled directly but instead $CO_{2(g)}$ was pumped into the bottle headspace, such as describe in a recent published laboratory culture study on coccolithophores (Phelps et al., 2021). In their 2.5 L volume vessels of 1 L approximately 2000 µM DIC, the isotopic difference between CO_2 tank and the natural seawater medium was not reported. Given natural seawater, the carbon isotope of DIC was likely in the range of 1 to 1.6‰ (Bidigare et al., 1997). Typical standard commercial CO_2 gas cylinders produced from fossil fuel combustion around -37‰. The range of carbon isotope difference would be ~38‰ and the expected equilibrium $\delta^{13}C_{DIC}$ value after bubbling would be about -29‰. Measurement of $\delta^{13}C_{DIC}$ at the start and end of the 5 day duration of experiment showed the least negative values (-7 to -9‰) in the 200 ppm CO_2 treatment and the most negative values (-15 to -17‰) in the 1000 ppm treatment (see Figure S8 in Phelps et al. (2021)). As the gas exchange rate constant should be the same between treatments, the gas exchange rate increases with the CO_2 concentration (see the **Eq. 2** in **Section 3**). This would lead to the DIC carbon isotope value in the 1000 ppm treatment being

closer to equilibrium (more negative) than that in the 200 ppm CO_2 experiment. In this study, in order to minimize the impact of evolving $\delta^{13}C_{DIC}$, the isotopic fractionation was calculated using the final DIC carbon isotope ratio of each experiment, as representative of the DIC in which most of the harvested culture biomass was produced. Therefore, in this case, even if the DIC carbon isotope ratios did not reach equilibrium with the CO_2 gas, the fractionation results are still robust with help of DIC measurements. However, the disequilibrium between DIC and $CO_{2(g)}$ could add additional errors in ε_p calculations, because of the gradual negative shift of DIC carbon isotope over the course of the culture. Additionally, the carbon isotope exchange rate would be faster when there is more disequilibrium with $CO_{2(g)}$, resulting a larger potential error in ε_p estimations (**Figure 5a**). In conclusion, even if the DIC carbo isotope ratios are measured carefully, it is still more optimal to ensure isotopic equilibrium in DIC for a stable $\delta^{13}C_{DIC}$ to reduce the potential error.

5.2.2 Active bubbling of batch cultures

Shorter equilibration times would be expected in the cultures which are actively bubbled compared to culture with only gas surface aeration. Remize et al. (2021) actively bubbled 2 L culture vessels of natural seawater of initially 750 µM DIC with an intensity of 5 bubbles per second. The isotopic difference between the CO_2 tank (-37.7‰) and natural seawater media (5‰) of would be 42‰ and the expected equilibrium value after bubbling would be ~-30.5‰ at T_k = 292K. Measurement of $\delta^{13}C_{DIC}$ every 4 days reveals $\delta^{13}C_{DIC}$ attained -31‰, the expected equilibrium value after around 20 days. The equilibration likely required >10 days due to a slow gas exchange rate resulting from low-intensity bubbling and low CO_2 concentration. The $\delta^{13}C$ of biomass sampled every 4 days throughout the experiment also evolves by 40‰ in parallel with the evolution of the $\delta^{13}C_{DIC}$.

Another example using bubbling method is Liu et al. (2018), who studied the carbon isotopic fractionation of a coastal coccolithophore, *Ochrosphaera neapolitana*. However, instead of measuring DIC carbon isotope ratios directly, they calculated expected DIC carbon isotope ratios assuming equilibrium with $CO_{2(g)}$. Their carbon isotope fractionation results, in both calcite and organic carbon, were higher than other coccolithophores laboratory culture results (Hermoso et al., 2016; Rickaby et al., 2010; Stoll et al., 2019) by ~5–10‰. Moreover, they bubbled the DIC in three different CO_2-level groups by gas with three different carbon isotope ratios ranging from -15‰ to -37‰. This could cause differences in the extent of isotopic disequilibrium among the experiments, as shown in **Figure 4c** and **Figure 5b**.

5.2.3 Bubbling in continuous culture setups

More complex situations arise with continuous culturing set-up. An example would be bubbling of the culture vessel but not the inflow bottle, from which new medium is pumped into the culture for (semi-)continuous dilution (Wilkes et al., 2017; Wilkes et al., 2018). In this system, the CO_2 added was -38.6‰ for all cultures, and natural seawater (assumed to be about 1 to 1.6‰ as Bidigare et al. (1997)), in a 4 L culture vessel. The expected equilibrium $\delta^{13}C_{DIC}$ would be -30‰. Different dilution rates were employed to control algae growth rate. In such a system the DIC carbon isotope could be closer to equilibrium when the dilution rate is lower. From the observations, it appears that the DIC in high CO_2 and low dilution rates treatments get closest to equilibrium (from the Table 1 in Wilkes et al. (2017)), while the faster dilution rate and lower CO_2 are furthest from equilibrium (**Figure 5c**). Previous authors (Wilkes et al., 2017) suggested that differences in the bubbling regimen may have contributed to the very different results from continuous cultures of Hoins et al. (2016). In Hoins et al. (2016), the biomass carbon isotope fractionation shows a much more narrow range, only from 9 to 12‰, compared to the 14 to 26 ‰ in Wilkes et al. (2017), even though the CO_2 settings and cell growth rates in these two studies are similar. However, insufficient details are provided in the method of Hoins et al. (2016) to evaluate the role that isotopic equilibrium may have played in these divergent results, while the DIC carbon isotope ratios in Wilkes et al. (2017) were measured making the fractionation results more reliable.

Continuous cultures with faster equilibration are expected to result from using gas and medium with a $CO_{2(g)}$ to DIC isotopic difference around -9 to -8‰ (varying with temperature), as discussed in **Section 5.1**. Tchernov et al. (2014) described a culture in which natural seawater in Gulf of Maine, ~1.2‰ at nearest station in GLODAP V2 (Olsen et al., 2016), was bubbled with atmospheric CO_2 (~ -8.5‰), using, with expected equilibrium ranging from -7.6‰ at 26°C and -9.6‰ at 8°C (more equilibrium fractionations in different temperature can be found in **Appendix C**). The $CO_{2(g)}$ and DIC were close to reach isotopic equilibrium in this study. Therefore, although only the culture vessel not the media reservoir was bubbled, the equilibration time would have been very short (as seen in **Figure 4c**).

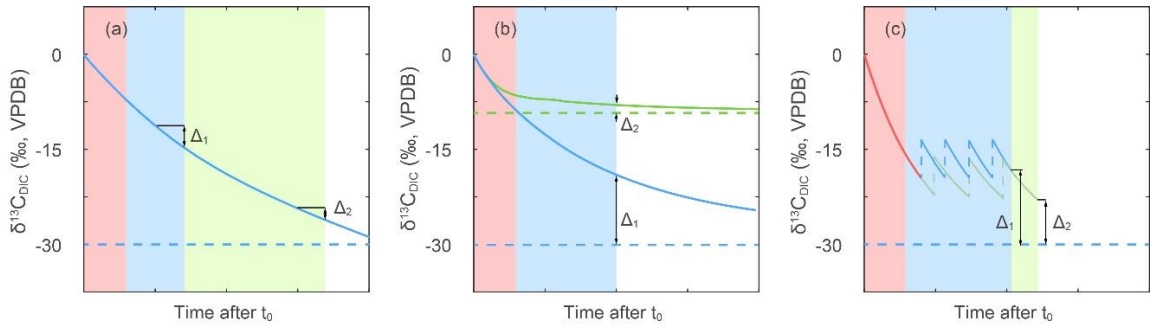

Figure 5. Concept model of isotopic disequilibrium effects in different experimental setups. Time advances from left to right in unspecified units since actual equilibration timescales depend on vessel dimensions and bubbling rate and surface area. Red shading areas represent the period in which media was bubbled before addition of cells. Blue and green shaded areas represent culture duration with bubbling. Horizontal dashed lines represent the $\delta^{13}C_{DIC}$ after reaching equilibrium with $CO_{2(g)}$, while solid lines give the time varying $\delta^{13}C_{DIC}$ for different scenarios detailed below. Blue lines are shown for the common situation of bubbling a media of initial $\delta^{13}C_{DIC}$ close to surface seawater (~0‰) with $CO_{2(g)}$ of ~-38 ‰. The Δ_1 and Δ_2 are used to illustrate potential errors in estimation of $\delta^{13}C_{DIC}$, as detailed below. **(a)** Potential effect of the timing of sampling on the uncertainty in the $\delta^{13}C_{DIC}$. Because cells are produced not only the last day, but also a period of time before harvest, if the $\delta^{13}C_{DIC}$ at time of cell harvest time was employed in fractionation calculation, the more rapid $\delta^{13}C_{DIC}$ evolution early in the experiment could lead to a larger error as (Δ_1 vs Δ_2). Different CO_2 concentration treatments with different rates of reaching equilibrium, or different culture durations can cause differences in error as well as bias the estimation of $\delta^{13}C_{DIC}$ corresponding to period of cell production. **(b)** Comparison of the effect of $\delta^{13}C_{CO2(g)}$ of -38‰ (blue lines) vs ~-17‰ (green lines) on estimation of $\delta^{13}C_{DIC}$. The DIC carbon isotope would reach equilibrium faster with a $CO_{2(g)}$ to DIC isotopic difference of around -8.3‰ leading to a smaller disequilibrium. This effect could be more serious when the DIC carbon isotope ratios are not measured. **(c)** The effect of dilution frequency on DIC carbon isotope evolution in continuous culturing set-ups. Blue and green lines present two different dilution treatments and red line represents $\delta^{13}C_{DIC}$ evolution before first dilution. The vertical dashed lines represent positive shifts in carbon isotope caused by dilutions with un-bubbled seawater. Higher dilution rate would lead to a larger disequilibrium as Δ_1, if the seawater reservoir is not pre-bubbled to equilibrium with $CO_{2(g)}$, which could also increase the error of fractionations in continuous culture set-ups.

5.3 Suggestions for future studies

As discussed in the previous section, isotopic disequilibrium is likely to have happened widely in current carbon isotopic studies involving bubbling of cultures. Most ocean acidification

studies did check the ordinary chemistry equilibrium carefully by monitoring the seawater pH or DIC concentration during bubbling. But the carbon isotopic equilibrium has often been ignored so far, which could be much slower than the ordinary equilibrium. Here we suggest that for all laboratory culture works on carbon isotope fractionation, measuring the DIC carbon isotope ratio directly is always very necessary, at least once at the beginning and again the end of culture, in case the DIC is in disequilibrium with $CO_{2(g)}$. We can estimate the isotope ratio at equilibrium quickly by $\delta^{13}C_{CO2(g)} - \Delta_{eq}$, where Δ_{eq} is the equilibrium carbon isotope fractionation between $CO_{2(g)}$ and DIC (defined as $\delta^{13}C_{CO2(g)}$- $\delta^{13}C_{DICeq}$, ~-8.3 when the temperature is about 291.15K and pH is around 7.8-8.2 in this study). The Δ_{eq} for different temperature and pH combinations have been listed in **Table C1**. If regular DIC carbon isotope measurements are not available, a safe solution could be pre-bubbling seawater for more than one week before carrying out any culture experiments. Even with measurements of DIC carbon isotope ratios, we still recommend that the DIC carbon isotope should reach (or close to) isotopic equilibrium with $CO_{2(g)}$, to minimize the error in carbon isotope fractionation calculations. For continuous culture, the media reservoir used for dilution should also be pre-bubbled to avoid huge carbon isotope shift during culture, which can also reduce the error. We also suggest that, it is necessary to report, as detailed as possible, the culture methods, including the $CO_{2(g)}$ carbon isotope ratio, initial DIC carbon isotope ratio, pre-bubbling duration, dilution percentage, for the benefits of data comparison in future works.

For a chemostat system similar with the photobioreactor system employed in this work, both the ordinary and isotopic equilibriums are primarily limited by the CO_2 exchange rate between the gas phase and liquid phase. As discussed in the sensitivity test results, increasing the k_E can significantly accelerate equilibration process. Firstly, exchange rate can be accelerated by increasing the gas flux. However, some large or fragile phytoplankton species, such as *Trichodesmium erythraeum* and dinoflagellate species, might be affected by the turbulence caused by bubbling (Hurd et al., 2009). Therefore, most studies employed a 'gentle bubbling', with a gas flux ranging from 100 ml min^{-1} to 300 ml min^{-1} for culture flasks in a few liters (e.g. Gordillo et al., 2015; Li et al., 2012). Additionally, it was also recommended to stop bubbling for the first day of incubation as the algae get acclimated (Shi et al., 2009). In conclusion, we should avoid increasing the gas exchange rate by increasing the gas flux, especially for algae culture. Another way to accelerate equilibrium is using a gas-diffuser (also known as an air-stone), which could divide gas bubbles into larger number of smaller bubbles significantly increasing the surface area between gas phase and seawater phase. Gas diffusers of plastic or glass are likely to provide the best option for gas diffusion in culture.

For studies evaluating vital effect in the oxygen isotope ratios of carbonate shells, such as coccolith, the shells of foraminifera and bivalve, the oxygen isotope equilibrium between $CO_{2(g)}$ and water should be also considered. In theory, the oxygen isotope equilibrium should take longer to reach equilibrium than that of the carbon isotopes. This is because in a closed system, the equilibration time for carbon isotopes is only 10^2 seconds, but the equilibration time for oxygen isotopes is about a few hours (Zeebe and Wolf-Gladrow, 2001). Previously, the oxygen isotope issue was ignored because oxygen atom from water is dominated in a DIC-H_2O system. For example, in 1 L seawater with [DIC] = 2.3 mM and pH = 8.2, there are only about 4.6×10^{-3} mol oxygen atom derived from DIC but about 55 mol oxygen atoms from H_2O. However, continuous CO_2 bubbling will bring more oxygen atoms from $CO_{2(g)}$ into medium. This will alter the seawater oxygen isotope ratio if the oxygen isotope in $CO_{2(g)}$ is not naturally equilibrium with the oxygen isotope ratio of H_2O. Therefore, when biogenic carbonate oxygen isotope fractionation experiments are carried out using CO_2 bubbling, cautions are advised that the water oxygen isotope results could be influenced by disequilibrium among $CO_{2(g)}$-DIC-H_2O.

During culturing, the biomass consumes DIC and nutrients continually modifying the culture medium chemical and isotopic composition. Historically, previous work had to employ dilute batch cultures to avoid large shifts in both DIC concentration and isotopic composition. Chemostat systems were designed to keep a stable cell growth environment with help of numerical model (e.g. Ajbar and Alhumaizi, 2011). With cell density, growth rate, PIC and POC per cell, it would be possible to simulate how cell growth influences the DIC concentrations and isotope ratios evolution in continuous cultures, and very low cell density may no longer be the only way to achieve an accurate estimation of isotopic fractionation and stable carbonate system. Carbon isotope fractionation results in batch culture can also be re-calculated more accurately by employing an isotopic model to simulated a dynamic DIC carbon isotope ratio, than simply using the DIC carbon isotope ratio at the end of culture.

Appendix A. Notations of model

Table A1. Isotopic fractionation factors and reaction rate constants employed in simulations

Symbol	Meaning	Value	Reference and note
Reaction rate constant			
k_{+1}	Rate constant of CO_2 hydration (s^{-1})	$\ln k_{+1} = 1246.98 - \frac{61900}{T_k} - 183 \ln T_k$	Johnson (1982)
k_{-1}	Rate constant of HCO_3^- dehydration ($M\ s^{-1}$)	$k_{-1} = \frac{k_{+1}}{K1}$	K1 is the first dissociation constants of carbonic acid (Lueker et al., 2000)
k_{+4}	Rate constant of CO_2 hydroxylation ($M\ s^{-1}$)	$\ln k_{+4} = 17.67 - \frac{2790.47}{T_k}$	Johnson (1982)
k_{-4}	Rate constant of HCO_3^- hydroxylation (s^{-1})	$k_{-4} = k_{+4}\frac{K_w}{K1}$	K_w is stoichiometric ion product of water (Dickson and Goyet, 1994)
k_{+1}^{13}	Rate constant of $^{13}CO_2$ hydration (s^{-1})	$k_{+1}^{13} = \frac{k_{+1}}{1.013}$	O'leary et al. (1992)
k_{-1}^{13}	Rate constant of $H^{13}CO_3^-$ dehydration ($M\ s^{-1}$)	$k_{-1}^{13} = \frac{k_{-1}}{1.013\left(1 - \frac{\varepsilon_{CO2aq-HCO3}}{1000}\right)}$	$\varepsilon_{CO2aq-HCO3}$ is the equilibrium fractionation between $CO_{2(aq)}$ and HCO_3^-, varying with temperature (~9‰ at T_k = 291K, Zhang et al., 1995)
k_{+4}^{13}	Rate constant of $^{13}CO_2$ hydroxylation ($M\ s^{-1}$)	$k_{+1}^{13} = \frac{k_{+1}}{1.011}$	Zeebe (1999)
k_{-4}^{13}	Rate constant of $H^{13}CO_3^-$ dehydroxylation (s^{-1})	$k_{-4}^{13} = \frac{k_{-4}}{1.013\left(1 - \frac{\varepsilon_{CO2aq-HCO3}}{1000}\right)}$	
Isotopic fractionations			
α_{aq2g},α_{aq2g}	^{13}C fractionation in $CO_{2(aq)}$ exchanging with $CO_{2(g)}$	$\frac{\alpha_{aq2g}}{\alpha_{aq2g}} = 1 + \frac{\varepsilon_{CO2aq-CO2g}}{1000} = 0.99878$	$\varepsilon_{CO2aq-CO2g}$ is the equilibrium fractionation between $CO_{2(aq)}$ and $CO_{2(g)}$, varying with temperature (~-1.22 at T_k = 291K, Zhang et al., 1995)
α_{dif}	^{13}C fractionation in $CO_{2(g)}$ diffusion	0.9956	O'Leary (1988)
Other parameters			
XB1	Fraction of HCO_3^- in (HCO_3^- + CO_3^{2-})	$XB1 = \frac{1}{1 + \frac{K2}{[H^+]}}$	K2 is the second dissociation constants of carbonic acid (Lueker et al., 2000)
$X^{13}B1$	Fraction of $H^{13}CO_3^-$ in ($H^{13}CO_3^-$ + $^{13}CO_3^{2-}$)	$X^{13}B1 = \frac{1}{1 + \frac{K2}{[H^+]}\alpha_{CO3-HCO3}}$	$\alpha_{CO3-HCO3}$ is the carbon isotope fractionation between CO_3^{2-} and HCO_3^- (Zhang et al., 1995)

Appendix B: ODEs in model

$$\frac{dG_h}{dt} = k_{E1}\,(C_b\,k_H - G_h) + k_{E2}\,(C_p\,k_H - G_h) + F(G_g - G_h) \quad (Eq.B1)$$

$$\frac{d^{13}G_h}{dt} = k_{E1}\left({}^{13}C_b\,k_H\alpha_{aq2g} - {}^{13}G_h\,\alpha_{g2aq}\right) + k_{E1}\left({}^{13}C_p\,k_H\alpha_{aq2g} - {}^{13}G_h\,\alpha_{g2aq}\right) + F\left({}^{13}C_g\,\alpha_{dif} - {}^{13}G_h\,\alpha_{dif}\right) \text{(Eq. B2)}$$

$$\frac{dC_b}{dt} = \frac{k_{E1}}{V_b}(G_h - C_b\,k_H) + \left(k_{-1}H_b^+ + k_{-4}\right)C_b - \left(k_{+1} + k_{+4}\,OH_b^-\right)B_b\,XB1_b \quad (Eq.B3)$$

$$\frac{d^{13}C_b}{dt} = \frac{k_{E1}}{V_b}\left({}^{13}G_h\,\alpha_{g2aq} - {}^{13}C_b\,k_H\alpha_{aq2g}\right) + \left(k_{+1}^{13} + k_{+4}^{13}\,OH_b^-\right){}^{13}B_b\,X^{13}B1_b - \left(k_{-1}^{13}H_b^+ + k_{-4}^{13}\right){}^{13}C_b \text{ (Eq. B4)}$$

$$\frac{dB_b}{dt} = -\left(k_{-1}H_b^+ + k_{-4}\right)C_b + \left(k_{+1} + k_{+4}\,OH_b^-\right)B_b\,XB1_b \quad (Eq.B5)$$

$$\frac{d^{13}B_b}{dt} = -\left(k_{-1}^{13}H_b^+ + k_{-4}^{13}\right){}^{13}C_b + \left(k_{+1}^{13} + k_{+4}^{13}\,OH_b^-\right){}^{13}B_b\,X^{13}B1_b \quad \text{(Eq. B6)}$$

$$\frac{dC_p}{dt} = \frac{k_{E2}}{V_p}\left(G_h - C_p\,k_H\right) + \left(k_{-1}H_p^+ + k_{-4}\right)C_p - \left(k_{+1} + k_{+4}\,OH_p^-\right)B_p\,XB1_p \quad \text{Eq(B7)}$$

$$\frac{d^{13}C_p}{dt} = \frac{k_{E2}}{V_p}\left({}^{13}G_h\,\alpha_{g2aq} - {}^{13}C_p\,k_H\alpha_{aq2g}\right) + \left(k_{+1}^{13} + k_{+4}^{13}\,OH_p^-\right){}^{13}B_p\,X^{13}B1_p - \left(k_{-1}^{13}H_p^+ + k_{-4}^{13}\right){}^{13}C_p \,(Eq.B8)$$

$$\frac{dB_p}{dt} = -\left(k_{-1}H_p^+ + k_{-4}\right)C_p + \left(k_{+1} + k_{+4}\,OH_p^-\right)B_p\,XB1_p \quad (Eq.B9)$$

$$\frac{d^{13}B_p}{dt} = -\left(k_{-1}^{13}H_p^+ + k_{-4}^{13}\right){}^{13}C_p + \left(k_{+1}^{13} + k_{+4}^{13}\,OH_p^-\right){}^{13}B_p\,X^{13}B1_p \quad (Eq.B10)$$

where capital letters G, C, B, H and OH represent $CO_{2(g)}$, $CO_{2(aq)}$, HCO_3^-+CO_3^{2-}, H^+ and OH^-, respectively. and subscript letters, h, b and p, are headspace, bottle and photobioreactor, respectively. The V means volume. The descriptions of reaction rate constants, isotopic fractionation and other parameters can be found in **Table A1**.

Appendix C: Equilibrium isotopic fractionation between $CO_{2(g)}$ and DIC in different temperature and pH

The equilibrium isotopic fractionation between $CO_{2(g)}$ and DIC (Δ_{eq}) is defined as $\delta^{13}C_{CO2(g)} - \delta^{13}C_{DIC}$. In the Section 5.1, it has been shown that when the $\Delta_{t=0}$ is equal with or more negative than Δ_{eq}, the isotopic equilibrium could be reached very fast. The Δ_{eq} is mainly controlled by temperature and slightly influenced by pH. Here we calculate Δ_{eq} in different temperature and pH combinations by the equilibrium fractionation between different DIC compositions (Zeebe and Wolf-Gladrow, 2001; Zhang et al., 1995).

Table C1. The equilibrium carbon isotope fractionation between $CO_{2(g)}$ and DIC (Δ_{eq}) in different temperatures and pH.

T(°C) / pH	5	10	15	20	25
7.5	-9.671	-9.205	-8.716	-8.211	-7.692
7.6	-9.678	-9.210	-8.721	-8.214	-7.695
7.7	-9.684	-9.215	-8.725	-8.218	-7.699
7.8	-9.691	-9.221	-8.730	-8.223	-7.703
7.9	-9.698	-9.227	-8.736	-8.228	-7.708
8	-9.705	-9.234	-8.742	-8.234	-7.713
8.1	-9.714	-9.243	-8.750	-8.241	-7.719
8.2	-9.726	-9.253	-8.759	-8.249	-7.726
8.3	-9.741	-9.265	-8.771	-8.259	-7.735
8.4	-9.758	-9.281	-8.782	-8.270	-7.744
8.5	-9.779	-9.299	-8.798	-8.282	-7.754

Declaration of Competing Interest

The authors declare that they have no known competing financial interests or personal relationships that could have appeared to influence the work reported in this paper

Author contributions

IT and HZ carried out the bubbling experiments. IT and PA measured carbon isotope with help from MJ in data calibration. HZ developed the numerical model. HZ and HMS wrote the paper with input from other authors.

Acknowledgement

This study was supported by the Swiss National Science Foundation (Award 200021_182070) and ETH Zurich (ETH03-19-1).

Data section

All measurements are listed in Table 1-3. The model is in Appendix B.

References

Ajbar, A. and Alhumaizi, K. (2011) Dynamics of the chemostat: a bifurcation theory approach. CRC Press.

Bidigare, R.R., Fluegge, A., Freeman, K.H., Hanson, K.L., Hayes, J.M., Hollander, D., Jasper, J.P., King, L.L., Laws, E.A., Milder, J., Millero, F.J., Pancost, R., Popp, B.N., Steinberg, P.A. and Wakeham, S.G. (1997) Consistent fractionation of 13C in nature and in the laboratory: Growth-rate effects in some haptophyte algae. Global Biogeochemical Cycles 11, 279-292.

Carroll, J.J., Slupsky, J.D. and Mather, A.E. (1991) The solubility of carbon dioxide in water at low pressure. Journal of Physical and Chemical Reference Data 20, 1201-1209.

Dickson, A.G. and Goyet, C. (1994) Handbook of methods for the analysis of the various parameters of the carbon dioxide system in sea water. Version 2. Oak Ridge National Lab., TN (United States).

Figuerola, B., Hancock, A.M., Bax, N., Cummings, V.J., Downey, R., Griffiths, H.J., Smith, J. and Stark, J.S. (2021) A review and meta-analysis of potential impacts of ocean acidification on marine calcifiers from the Southern Ocean. Frontiers in Marine Science 8, 24.

Gattuso, J.-P. and Hansson, L. (2011) Ocean acidification. Oxford University Press.

Gattuso, J.-P., Lee, K., Rost, B. and Schulz, K. (2010) Approaches and tools to manipulate the carbonate chemistry. Publications Office of the European Union.

Gordillo, F.J., Aguilera, J., Wiencke, C. and Jiménez, C. (2015) Ocean acidification modulates the response of two Arctic kelps to ultraviolet radiation. Journal of Plant Physiology 173, 41-50.

Hermoso, M., Chan, I.Z.X., McClelland, H.L.O., Heureux, A.M.C. and Rickaby, R.E.M. (2016) Vanishing coccolith vital effects with alleviated carbon limitation. Biogeosciences 13, 301-312.

Hoegh-Guldberg, O., Mumby, P.J., Hooten, A.J., Steneck, R.S., Greenfield, P., Gomez, E., Harvell, C.D., Sale, P.F., Edwards, A.J. and Caldeira, K. (2007) Coral reefs under rapid climate change and ocean acidification. science 318, 1737-1742.

560 Hoins, M., Eberlein, T., Grobetamann, C.H., Brandenburg, K., Reichart, G.J., Rost, B., Sluijs, A.
561 and Van de Waal, D.B. (2016) Combined Effects of Ocean Acidification and Light or Nitrogen
562 Availabilities on 13C Fractionation in Marine Dinoflagellates. PLoS One 11, e0154370.
563 Hopkinson, B.M., Dupont, C.L., Allen, A.E. and Morel, F.M.M. (2011) Efficiency of the CO2-
564 concentrating mechanism of diatoms. Proceedings of the National Academy of Sciences 108,
565 3830-3837.
566 Hurd, C.L., Beardall, J., Comeau, S., Cornwall, C.E., Havenhand, J.N., Munday, P.L., Parker,
567 L.M., Raven, J.A. and McGraw, C.M. (2019) Ocean acidification as a multiple driver: how
568 interactions between changing seawater carbonate parameters affect marine life. Marine
569 and Freshwater Research 71, 263-274.
570 Hurd, C.L., Hepburn, C.D., Currie, K.I., Raven, J.A. and Hunter, K.A. (2009) Testing the effects
571 of ocean acidification on algal metabolism: considerations for experimental designs 1.
572 Journal of Phycology 45, 1236-1251.
573 Iglesias-Rodriguez, M.D., Halloran, P.R., Rickaby, R.E., Hall, I.R., Colmenero-Hidalgo, E.,
574 Gittins, J.R., Green, D.R., Tyrrell, T., Gibbs, S.J. and von Dassow, P. (2008) Phytoplankton
575 calcification in a high-CO2 world. science 320, 336-340.
576 Johnson, K.S. (1982) Carbon dioxide hydration and dehydration kinetics in seawater 1.
577 Limnology and Oceanography 27, 849-855.
578 Keller, M.D., Selvin, R.C., Claus, W. and Guillard, R.R. (1987) Media for the culture of oceanic
579 ultraphytoplankton 1, 2. Journal of phycology 23, 633-638.
580 Lemasson, A.J., Fletcher, S., Hall-Spencer, J.M. and Knights, A.M. (2017) Linking the biological
581 impacts of ocean acidification on oysters to changes in ecosystem services: a review. Journal
582 of Experimental Marine Biology and Ecology 492, 49-62.
583 Li, W., Gao, K. and Beardall, J. (2012) Interactive effects of ocean acidification and nitrogen-
584 limitation on the diatom Phaeodactylum tricornutum. PloS one 7, e51590.
585 Liu, Y.W., Eagle, R.A., Aciego, S.M., Gilmore, R.E. and Ries, J.B. (2018) A coastal
586 coccolithophore maintains pH homeostasis and switches carbon sources in response to
587 ocean acidification. Nat Commun 9, 2857.
588 Lueker, T.J., Dickson, A.G. and Keeling, C.D. (2000) Ocean pCO2 calculated from dissolved
589 inorganic carbon, alkalinity, and equations for K1 and K2: validation based on laboratory
590 measurements of CO2 in gas and seawater at equilibrium. Marine Chemistry 70, 105-119.
591 Martínez, I. and Casas, P. (2012) Simple model for CO2 absorption in a bubbling water
592 column. Brazilian Journal of Chemical Engineering 29, 107-111.
593 Meyer, J. and Riebesell, U. (2015) Reviews and Syntheses: Responses of coccolithophores to
594 ocean acidification: a meta-analysis. Biogeosciences 12, 1671-1682.
595 Mills, G.A. and Urey, H.C. (1940) The kinetics of isotopic exchange between carbon dioxide,
596 bicarbonate ion, carbonate ion and water1. Journal of the American Chemical Society 62,
597 1019-1026.
598 Mostofa, K.M., Liu, C.-Q., Zhai, W., Minella, M., Vione, D., Gao, K., Minakata, D., Arakaki, T.,
599 Yoshioka, T. and Hayakawa, K. (2016) Reviews and Syntheses: Ocean acidification and its
600 potential impacts on marine ecosystems. Biogeosciences 13, 1767-1786.
601 Nishida, K., Chew, Y.C., Miyairi, Y., Hirabayashi, S., Suzuki, A., Hayashi, M., Yamamoto, Y.,
602 Sato, M., Nojiri, Y. and Yokoyama, Y. (2020) Novel reverse radioisotope labelling experiment
603 reveals carbon assimilation of marine calcifiers under ocean acidification conditions.
604 Methods in Ecology and Evolution 11, 739-750.
605 O'leary, M., Madhavan, S. and Paneth, P. (1992) Physical and chemical basis of carbon
606 isotope fractionation in plants. Plant, Cell & Environment 15, 1099-1104.
607 O'Leary, M.H. (1988) Carbon Isotopes in Photosynthesis. BioScience 38, 328-336.
608 Olsen, A., Key, R.M., Van Heuven, S., Lauvset, S.K., Velo, A., Lin, X., Schirnick, C., Kozyr, A.,
609 Tanhua, T. and Hoppema, M. (2016) The Global Ocean Data Analysis Project version 2

(GLODAPv2)–an internally consistent data product for the world ocean. Earth System Science Data 8, 297-323.
Phelps, S.R., Hennon, G.M.M., Dyhrman, S.T., Hernández-Limón, M.D., Williamson, O.M. and Polissar, P.J. (2021) Carbon Isotope Fractionation in Noelaerhabdaceae Algae in Culture and a Critical Evaluation of the Alkenone Paleobarometer. Geochemistry, Geophysics, Geosystems.
Remize, M., Planchon, F., Loh, A.N., Le Grand, F., Mathieu-Resuge, M., Bideau, A., Corvaisier, R., Volety, A. and Soudant, P. (2021) Fatty acid isotopic fractionation in the diatom Chaetoceros muelleri. Algal Research 54.
Rickaby, R.E.M., Henderiks, J. and Young, J.N. (2010) Perturbing phytoplankton: response and isotopic fractionation with changing carbonate chemistry in two coccolithophore species. Clim. Past 6, 771-785.
Riebesell, U., Fabry, V.J., Hansson, L. and Gattuso, J.-P. (2011) Guide to best practices for ocean acidification research and data reporting. Office for Official Publications of the European Communities.
Riebesell, U. and Tortell, P.D. (2011) Effects of ocean acidification on pelagic organisms and ecosystems. Ocean acidification, 99-121.
Shi, D., Xu, Y. and Morel, F.M.M. (2009) Effects of the pH/pCO₂ control method on medium chemistry and phytoplankton growth. Biogeosciences 6, 1199-1207.
Stoll, H.M., Guitian, J., Hernandez-Almeida, I., Mejia, L.M., Phelps, S., Polissar, P., Rosenthal, Y., Zhang, H. and Ziveri, P. (2019) Upregulation of phytoplankton carbon concentrating mechanisms during low CO2 glacial periods and implications for the phytoplankton pCO2 proxy. Quaternary Science Reviews 208, 1-20.
Tchernov, D., Gruber, D.F. and Irwin, A. (2014) Isotopic fractionation of carbon in the coccolithophorid Emiliania huxleyi. Marine Ecology Progress Series 508, 53-66.
Wilkes, E.B., Carter, S.J. and Pearson, A. (2017) CO2-dependent carbon isotope fractionation in the dinoflagellate Alexandrium tamarense. Geochimica et Cosmochimica Acta 212, 48-61.
Wilkes, E.B., Lee, R.B.Y., McClelland, H.L.O., Rickaby, R.E.M. and Pearson, A. (2018) Carbon isotope ratios of coccolith–associated polysaccharides of Emiliania huxleyi as a function of growth rate and CO 2 concentration. Organic Geochemistry.
Zeebe, R.E. (1999) An explanation of the effect of seawater carbonate concentration on foraminiferal oxygen isotopes. Geochimica et Cosmochimica Acta 63, 2001-2007.
Zeebe, R.E. and Wolf-Gladrow, D. (2001) CO2 in seawater: equilibrium, kinetics, isotopes. Gulf Professional Publishing.
Zhang, J., Quay, P.D. and Wilbur, D.O. (1995) Carbon isotope fractionation during gas-water exchange and dissolution of CO2. Geochimica et Cosmochimica Acta 59, 107-114.